THE ROYAL SOCIETY

The chemical-gas dynamic mechanisms of pulsating detonation wave instability

By Mark Short[1], Ashwani K. Kapila[2] and J. J. Quirk[3]

[1] *Theoretical and Applied Mechanics, University of Illinois, Urbana, IL 61801, USA*
[2] *Department of Mathematical Sciences, Rensselaer Polytechnic Institute, Troy, NY 12180, USA*
[3] *Graduate Aeronautical Laboratories, Mail Code 205-45, California Institute of Technology, Pasadena, CA 91125, USA*

The chemical-gas dynamic mechanisms behind the instability and failure of a one-dimensional pulsating detonation wave driven by a three-step chain-branching reaction are revealed by direct numerical simulation. Two types of pulsating instability observed experimentally are explained. The first involves regular oscillations of the detonation front, where the instability is driven by low-frequency finite-amplitude compression and expansion waves in the chain-branching induction zone between the main reaction layer and the detonation shock. For irregular oscillations of the front, the instability mechanism first involves a decoupling between the shock and main reaction layer. Subsequently, the main reaction layer accelerates, drives a compression wave ahead of it, and undergoes a transition to detonation. This internal detonation wave overtakes the lead detonation shock, generating a new high-pressure detonation, which rapidly decays. A smaller-amplitude pressure oscillation occurs during the decay with a mechanism reminiscent of that observed for the previous regular oscillation, before the detonation and main reaction layer once again decouple and the instability cycle is repeated. For failure scenarios, the shock temperature is observed to drop to the cross-over temperature for the chain-branching reaction, causing the main reaction layer to decouple and retreat indefinitely from the detonation shock.

Keywords: detonations; instability; chain-branching reactions; failure

1. Introduction

Depending on the initial pressure, projectile velocity and mixture ratio of chemical reactant to diluent, two different regimes of pulsating detonation instability have been observed to occur when spherical or blunt-body objects are fired into a reactive atmosphere (Reugg & Dorsey 1963; Behrens *et al*. 1965; Cheryni 1968; Lehr 1972; McVey & Toong 1971; Alpert & Toong 1972; Kaneshige & Shepherd 1996). The first involves regular periodic oscillations of the flow field, while the second involves less regular but significantly larger-amplitude oscillations. Alpert & Toong (1972) refer to the former as the regular regime and the latter as the large disturbance regime. The large disturbance regime has also been observed in rectangular tubes by Saint-Cloud *et al*. (1972). In both cases, however, the characteristic hydrodynamic mechanisms of

the pulsating detonation instability are still poorly understood, despite the number of semiqualitative theories that have been put forward.

Two of the most plausible theories are those by McVey & Toong (1971) for regular pulsations and by Alpert & Toong (1972) for irregular pulsations. These are based on a semiqualitative analysis of the longitudinal oscillation which could arise within a square-wave detonation structure. Both theories are explained in detail by Fickett & Davis (1979) and involve a complicated wave interaction model, whereby a wave of compression overtakes the shock front generating a contact discontinuity in the process. The decrease in induction times in the high-temperature regime between the contact discontinuity and the shock front leads to a second reaction front (Short & Dold 1996) and a wave of compression which can again overtake the shock front and generate a new contact discontinuity. In the meantime, the collision of the two reaction fronts generates a forward-facing wave of expansion, which will overtake and weaken the strength of the main detonation shock. The timing of the latter process distinguishes the regular regime from the large-amplitude regime. Although semiqualitative, their model has gained widespread acceptance (Fickett & Davis 1979).

In the following, the mechanisms for both the regular and irregular modes of pulsating detonation wave instability are investigated by very-high-resolution direct numerical simulation. The chemistry is modelled by a three-step chain-branching reaction, having the distinct advantage over the standard one-step Arrhenius model of possessing a well-defined detonability limit (Short & Quirk 1997). The mechanisms driving both the instability and failure of the detonation wave are revealed by examining selected snapshot profiles of the thermodynamic and chemical structure behind the detonation shock during the unsteady evolution. The use of adaptive mesh refinement allows an effective resolution equivalent to 320 points in the standard steady-wave half-reaction length. We find that the mechanisms for both the regular regime and large-amplitude regime are found to differ from those proposed by McVey & Toong (1971) and Alpert & Toong (1972).

The results presented below demonstrate that regular pulsations arise due to the effects of low-frequency finite-amplitude compression and expansion wave propagation between the shock and main reaction layer. At a minimum point in the oscillatory detonation pressure cycle, a low-frequency wave of compression is generated, which connects the detonation shock to the main reaction layer, strengthens the shock front, subsequently decreasing the induction time and increasing the peak concentration of radical within the main reaction layer. The higher rate of energy release sustains the compression wave, until a maximum point in the detonation pressure cycle is reached, where the rate of heat release cannot sustain further increases in the shock pressure. The detonation shock then decays, resulting in a wave of expansion, which causes the main reaction to recede and the peak concentration of radical to decrease in amplitude until a minimum point in the detonation pressure cycle is reached and the oscillatory instability cycle is repeated.

The hydrodynamic mechanisms driving the large-amplitude irregular pulsations are substantially more complex. Here, two pressure modes are observed, one large amplitude and the other small amplitude. These give rise to the irregularity of the pulsation. The large-amplitude mode occurs when the main reaction layer and the shock front decouple, and the snapshot profile is that of a low-Mach-number fast-flame (Clarke 1983; Kassoy & Clarke 1985) held downstream of a detonation shock.

The flame accelerates, driving a wave of compression ahead of it. A transition to detonation then occurs, resulting in an internal detonation that overtakes the original detonation shock, generating a brief, but large, overpressure. This sequence is very reminiscent of the process of transition to detonation observed in the detonation initiation studies of Clarke *et al.* (1986, 1990), Sileem *et al.* (1991) and Dold *et al.* (1995). Here, though, the process of deflagration-to-detonation transition is found to be an integral part of the large-amplitude detonation instability mechanism. The detonation wave which results from the overtaking of the original shock by the internal detonation wave decays rapidly in amplitude, but then undergoes a small-amplitude pressure oscillation, whose mechanism is governed by a sequence almost identical to that of the regular pulsation described above. After the small-amplitude pressure cycle is complete, the main reaction layer recedes from the detonation shock, the reaction layer and shock decouple, and the two-pressure mode cycle is repeated.

Finally, the behaviour of the main reaction layer relative to the detonation shock front is investigated in cases where the detonability limit is reached for the present three-step chain-branching reaction model, i.e. when the detonation shock temperature drops to the chain-branching cross-over temperature. Since chain radicals can only then be generated at an exponentially small rate, the main reaction layer is observed to recede continuously from the detonation shock. In particular, no internal transition to detonation is observed to occur on the long time-scale of the calculation, and we conclude that the detonation wave has failed.

2. Model

The pulsating detonation instability is modelled by the one-dimensional non-dimensional reactive Euler equations (Short & Quirk 1997)

$$\frac{\mathrm{D}\rho}{\mathrm{D}t} + \rho\frac{\partial u}{\partial x^{\mathrm{l}}} = 0, \quad \frac{\mathrm{D}u}{\mathrm{D}t} + \rho^{-1}\frac{\partial p}{\partial x^{\mathrm{l}}} = 0, \quad \frac{\mathrm{D}e}{\mathrm{D}t} + p\frac{\mathrm{D}\rho^{-1}}{\mathrm{D}t} = 0, \tag{2.1}$$

where the variables ρ, u, p and e are the density, velocity, pressure and specific internal energy, respectively. The superscript 'l' refers to a laboratory coordinate system. A polytropic equation of state and an ideal thermal equation of state are assumed, where

$$e = \frac{p}{(\gamma-1)\rho} - q, \qquad T = p/\rho, \tag{2.2}$$

q represents the local chemical heat energy and T represents the temperature. The scales for the density, pressure, temperature and velocity are the steady-wave post-shock density, pressure, temperature and sound speed, respectively.

The chemical reaction is modelled by the three-step chain-branching reaction

$$\left.\begin{array}{lll} \text{initiation:} & \mathrm{F} \to \mathrm{Y}, & k_{\mathrm{I}} = \exp\left(\dfrac{1}{\epsilon_{\mathrm{I}}}\left(\dfrac{1}{T_{\mathrm{I}}} - \dfrac{1}{T}\right)\right), \\ \text{chain-branching:} & \mathrm{F} + \mathrm{Y} \to 2\mathrm{Y}, & k_{\mathrm{B}} = \exp\left(\dfrac{1}{\epsilon_{\mathrm{B}}}\left(\dfrac{1}{T_{\mathrm{B}}} - \dfrac{1}{T}\right)\right), \\ \text{chain-termination:} & \mathrm{Y} \to \mathrm{P}, & k_{\mathrm{C}} = 1, \end{array}\right\} \tag{2.3}$$

for fuel F, chain-radical Y and product P. The chain-initiation, chain-branching and chain-termination rate constants are given by k_{I}, k_{B} and k_{C}, respectively. The inverse

activation energy for the initiation reaction is $\epsilon_{\rm I}$ and for the chain-branching reaction is $\epsilon_{\rm B}$. The chain-initiation and chain-branching cross-over temperatures are given by $T_{\rm I}$ and $T_{\rm B}$, respectively, and are the values at which the chain-initiation and chain-branching rates are equal to the chain-termination rate. The reference time $\tilde{t}_c^*$ is such that the chain-termination rate constant is unity, i.e. $k_{\rm C} = 1$, with the reference length equal to $\tilde{t}_c^*$ times the sound speed immediately behind the steady detonation shock. Consumption equations for fuel and radical are

$$\frac{{\rm D}f}{{\rm D}t} = -r_{\rm I} - r_{\rm B}, \quad \frac{{\rm D}y}{{\rm D}t} = r_{\rm I} + r_{\rm B} - r_{\rm C}, \tag{2.4}$$

where

$$r_{\rm I} = f\exp\left(\frac{1}{\epsilon_{\rm I}}\left(\frac{1}{T_{\rm I}} - \frac{1}{T}\right)\right), \quad r_{\rm B} = \rho f y \exp\left(\frac{1}{\epsilon_{\rm B}}\left(\frac{1}{T_{\rm B}} - \frac{1}{T}\right)\right), \quad r_{\rm C} = y, \tag{2.5}$$

and f and y represent mass fractions of fuel and radical. The chemical energy q is defined as

$$q = Q(1-f) - (Q+R)y, \tag{2.6}$$

where $Q > 0$ represents the total chemical energy available in the unreacted mixture and R represents the amount of endothermic energy absorbed by the initiation and chain-branching reactions in breaking down the reactant F into the energetic radical Y. In order to mimic the typical reaction dynamics of chain-branching chemistry, in addition we assume that

$$T_{\rm I} > 1, \quad T_{\rm B} < 1, \quad \epsilon_{\rm I} \ll \epsilon_{\rm B} \ll 1, \quad R = 0. \tag{2.7}$$

In a shock-attached coordinate system,

$$X = x^{\rm l} + D_{\rm s}^* t, \tag{2.8}$$

the steady-wave variation is determined by the Rankine–Hugoniot conditions,

$$p^* = a + (1-a)(1-bq^*)^{1/2}, \quad u^* = \frac{(1-p^*)}{\gamma M_{\rm s}^*} + M_{\rm s}^*, \quad \rho^* = \frac{M_{\rm s}^*}{u^*}, \tag{2.9}$$

together with the first-order equations

$$f_{,X}^* = -(r_{\rm I}^* + r_{\rm B}^*)/u^*, \quad y_{,X}^* = (r_{\rm I}^* + r_{\rm B}^* - r_{\rm C}^*)/u^*, \tag{2.10}$$

where $D_{\rm s}^*$ is the steady detonation Mach number relative to the post-shock sound speed, and

$$M_{\rm s}^{*2} = \frac{(\gamma-1)D^{*2}+2}{2\gamma D^{*2} - (\gamma-1)}, \quad a = \frac{\gamma M_{\rm s}^{*2}+1}{(\gamma+1)}, \quad b = \frac{M_{\rm s}^{*2} 2\gamma(\gamma-1)}{(1-a)^2(\gamma+1)}. \tag{2.11}$$

Here, D^* is the detonation Mach number with respect to the preshock sound speed, while $M_{\rm s}^*$ is the steady flow Mach number immediately behind the shock. The steady variables satisfy the shock conditions

$$\rho^* = p^* = T^* = 1, \quad u^* = M_{\rm s}^*, \quad f^* = 1, \quad y^* = 0. \tag{2.12}$$

Figure 1 shows the steady-state variation through the detonation for the three values of the chain-branching cross-over temperature used in the following study. The other

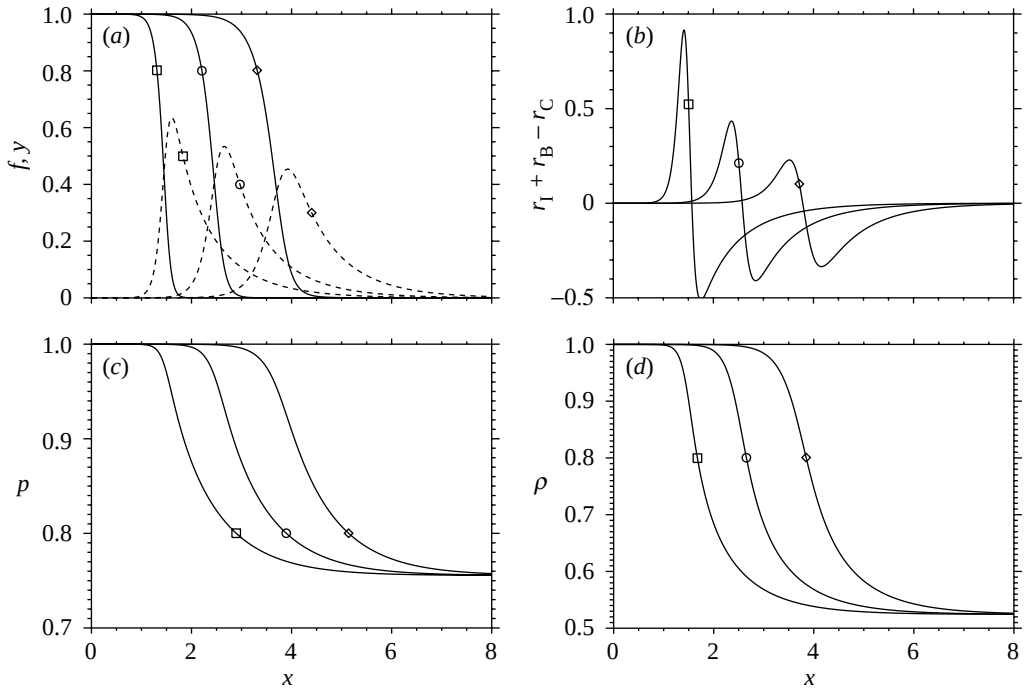

Figure 1. Steady detonation profiles showing: (*a*) fuel, f (solid lines) and radical, y (dashed lines); (*b*) radical production rate $r_\mathrm{I} + r_\mathrm{B} - r_\mathrm{C}$; (*c*) pressure p; (*d*) density ρ. The symbols mark corresponding profiles for the chain-branching cross-over temperatures $T_\mathrm{B} = 0.82$ (□), $T_\mathrm{B} = 0.86$ (○) and $T_\mathrm{B} = 0.89$ (◊).

parameters used in the study are those from Short & Quirk (1997), i.e. $Q = 3$, $\epsilon_\mathrm{I} = \frac{1}{20}$, $\epsilon_\mathrm{B} = \frac{1}{8}$, $T_\mathrm{I} = 3$, $\gamma = 1.2$ and overdrive $d = 1.2$. The overdrive d is defined as $d = (D^*/D^*_\mathrm{CJ})^2$, where D^*_CJ is the Chapman–Jouguet detonation velocity. Some asymptotic estimates of the ranges of chain-branching induction length in the steady structure are given in Short & Quirk (1997), but it should be noted that one could, in principle, derive several possible structures under the ordered limits allowed by the parameters in (2.7).

The gas dynamic mechanisms of the pulsating detonation instability are revealed by a direct numerical simulation of the model equations (2.1)–(2.3) with the state and rate equations (2.5)–(2.7) by employing an adaptive mesh refinement procedure (Quirk 1994, 1996) and a finite volume integration scheme based on Roe's linearized Riemann solver (Glaister 1988). For the simulations shown below, the computational grid was discretized using a uniform mesh of 8000 cells. Three extra subgrid levels were used, each with a refinement factor of 4, giving an effective resolution of 512 000 cells, or *ca.* 320 points per steady half-reaction length, on a uniform mesh. All computations were performed with a CFL number of 0.5. A presmeared shock was grafted onto the initial steady travelling wave in order to eliminate the start-up errors that are endemic to all shock-capturing schemes, so that initial perturbations to the wave were generated by small-amplitude disturbances arising from the truncation error of the integration scheme.

The clear necessity for such high levels of grid resolution are apparent from the

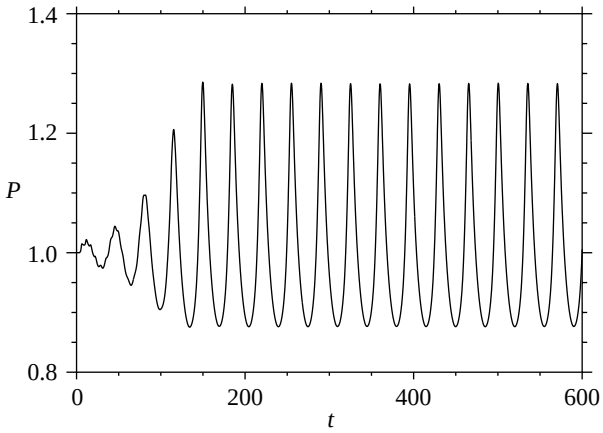

Figure 2. Shock pressure history for $T_{\mathrm{B}} = 0.82$.

snapshot profiles of the pulsating instability mechanisms shown below. While a resolution of, say, 40 points per half-reaction length might seem adequate to resolve the steady structure, the computation for $T_{\mathrm{B}} = 0.86$ illustrates the very fine spatial and temporal structures that can arise during the pulsation of the detonation front. Failure to resolve these structures can easily lead to a misleading interpretation of the instability mechanisms.

3. Regular pulsating instability

(*a*) *Regular mode: chain-branching cross-over temperature* $T_{\mathrm{B}} = 0.82$

Figure 2 shows the detonation shock pressure history for $T_{\mathrm{B}} = 0.82$. A linear stability analysis with $T_{\mathrm{B}} = 0.82$ (Short & Quirk 1997) establishes the presence of a single unstable oscillatory mode α_1 with a growth rate $\mathrm{Re}(\alpha_1) = 0.0235$ and period $T = 34.83$. The nonlinear numerical solution reveals a single-mode low-frequency oscillation with amplitude $A = 0.407$ and period $T = 35.0$. The oscillation has a maximum pressure peak $P = 1.283$ and minimum pressure point $P = 0.876$. This mode of instability observed in experiments is referred to as the regular mode by Alpert & Toong (1972). For a point of reference, the steady wave structure for $T_{\mathrm{B}} = 0.82$ has the shortest temperature-sensitive chain-branching induction zone of the three cases studied (figure 1).

Figure 3*b–e* reveals the gas dynamic mechanisms driving the regular longitudinal pulsating instability for $T_{\mathrm{B}} = 0.82$ during one cycle of the oscillation. Respectively, figure parts 3*b–e* represent snapshot profiles of pressure, density, radical mass fraction and radical production rate behind the detonation shock shown in a coordinate system (x) attached to the shock ($x = 0$). Figure 3*a* shows the stages in the cycle at which the snapshots are taken. The circles in figure 3*b–e* indicate the points of peak radical concentration, and reveal the position of the main heat-release layer relative to the detonation shock.

At the minimum point in the cycle, indicated by location 1 in figure 3*a*, the detonation shock pressure is $P = 0.876$ compared with the steady shock pressure $P = 1$. The peak radical concentration $y = 0.562$ lies at $x = -3.02$, compared with a peak $y = 0.635$ at $x = -1.61$ for the steady wave. The peak rate of radical production

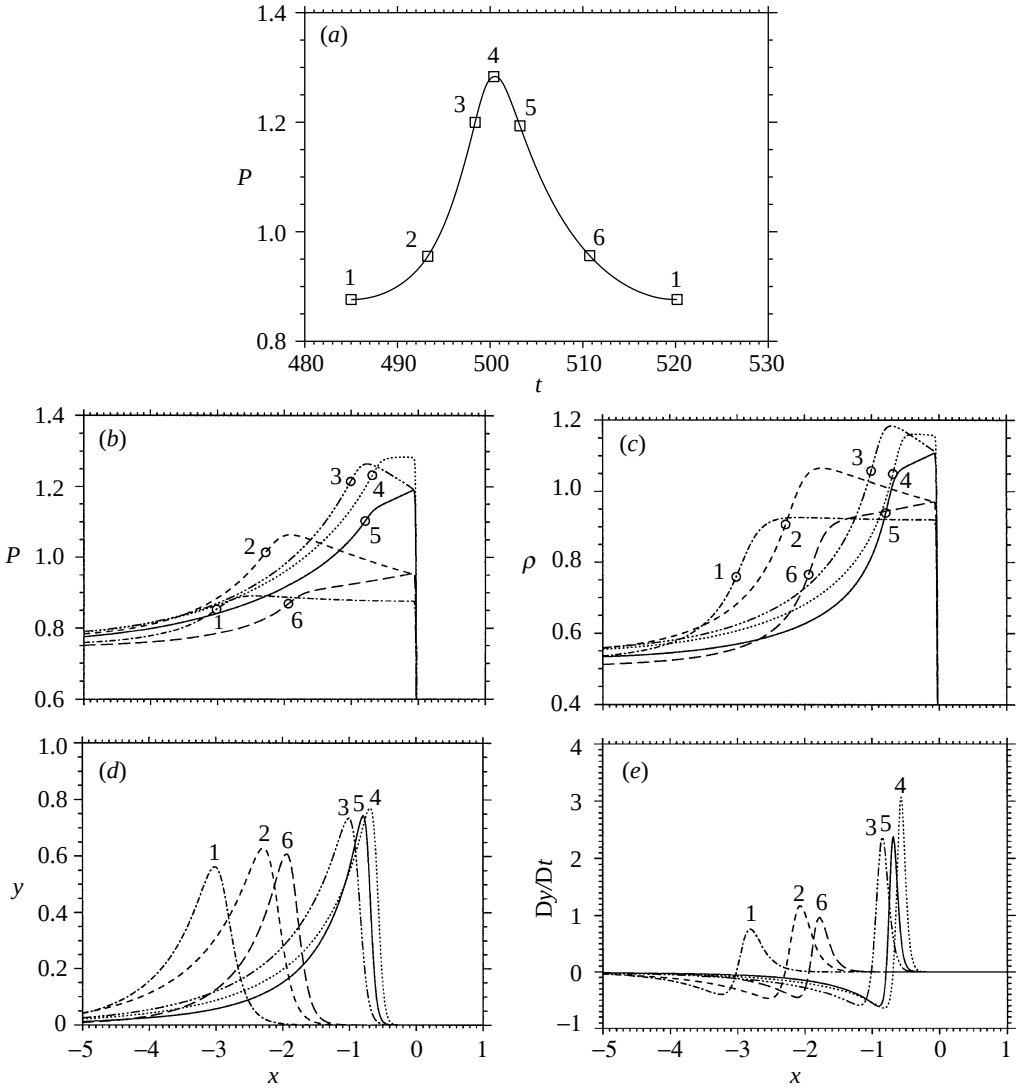

Figure 3. (*a*) Points in the detonation shock pressure cycle at which the snapshot profiles of the variation in (*b*) pressure, (*c*) density, (*d*) radical mass fraction and (*e*) radical production rate, shown in a frame of reference attached to the detonation shock, are taken during one cycle of the regular pulsating instability. These points correspond to the numerically labelled profile curves in (*b*)–(*e*). The circles in (*b*) and (*c*) correspond to the points of peak radical concentration.

$r_{\mathrm{I}}+r_{\mathrm{B}}-r_{\mathrm{C}}=0.753$ lies at $x=-2.81$, compared with a peak rate $r_{\mathrm{I}}+r_{\mathrm{B}}-r_{\mathrm{C}}=0.920$ at $x=-1.41$ for the steady wave. At this point in the cycle, the detonation structure consists of a long chain-branching induction region in which the pressure and density distributions are almost uniform. The pressure change through the main heat release layer is comparatively small relative to the corresponding change in the steady wave, whereas the density change remains significant. Thus the detonation structure at location 1 is reminiscent of a low-Mach-number fast-flame (Clarke 1983; Kassoy & Clarke 1985) held downstream of a normal shock wave with instantaneous Mach

number $D = 2.30$ relative to the upstream sound speed. However, this configuration is necessarily unsteady, since no steady solution having such weak pressure variation through the main reaction layer is possible for finite detonation propagation Mach numbers.

Unable to adopt a steady travelling-wave configuration, the next stage in the cycle, location 2 in figure 3*b–e*, shows a long-wavelength finite-amplitude compression wave formed within the induction zone, communicating changes in the main reaction layer structure to the shock front. During the time period $t = 8.27$ from location 1 to 2, the compression wave has amplified the shock pressure to $P = 0.955$. Large variations in induction-zone pressure and density have also appeared. The pressure drop through the main reaction layer is now significant. Thus, as a result of the rise in shock pressure and temperature, the chain-branching induction rate at the shock increases, accelerating the main reaction layer towards the shock. The instantaneous Mach number of the shock at location 2 is $D = 2.40$.

The accelerated rate of chemical energy release associated with the increase in shock pressure sustains the compression wave, and, at location 3 in the cycle, the shock pressure is $P = 1.195$, above that corresponding to the steady detonation value $P = 1$. The detonation structure now consists of a short chain-branching induction region relative to the steady structure, and a chain-recombination region that is much longer than the chain-induction zone. Thus, in contrast to its behaviour at location 1, the detonation structure at location 3 resembles that associated with a steady wave having a higher value of the chain-branching cross-over temperature T_{B} (Short & Quirk 1997). Large-amplitude pressure and density variations through the induction zone and main heat release layer remain present. The instantaneous shock Mach number at location 3 is $D = 2.68$.

The profiles at location 4 in figure 3*b–e* reveal the detonation structure at the completion of the amplification portion of the oscillatory cycle, where the detonation shock pressure has peaked, and, presumably, the degree of chemical energy release can no longer support further increases in the shock pressure. There is a short chain-branching induction zone at location 4, with the pressure and density distributions being again almost uniform in this region (cf. location 1). Following the short induction zone is the longest chain-recombination zone of the four profiles examined thus far. Both the maximum rate of radical production and peak concentration of radical are at their greatest at this stage in the cycle, with the peak radical concentration being $y = 0.770$ at $x = -0.69$ and the peak rate of radical production $r_{\mathrm{I}} + r_{\mathrm{B}} - r_{\mathrm{C}} = 3.067$ at $x = -0.57$. Again, there is a large pressure and density drop through the main reaction layer. The drop in pressure through the main reaction layer from the point of peak concentration to the point where $y = 0.05$ is 0.409, while the corresponding density change over the same region is 0.471. The instantaneous shock Mach number at location 4 has increased to $D = 2.78$.

After reaching its peak pressure in the cycle, the detonation shock starts to decay. Location 5 corresponds to an early stage in the decay cycle. Corresponding profiles for pressure and density indicate that an expansion wave with a wavelength commensurate with the chain-branching induction zone is the reason for the erosion. At location 5, the chain-branching induction zone consists of a region of finite expansion in which pressure and density drop significantly in the induction zone. Figure 3*d*, *e* demonstrates that the main reaction layer begins to recede from the shock front. The maximum rate of radical production also falls significantly from its value at location 4

and the peak radical concentration has a lower value $y = 0.742$ at $x = -0.79$. The instantaneous shock Mach number at location 5 has declined to $D = 2.68$.

The expansion wave continuously erodes into the detonation shock pressure and at location 6 has a value $P = 0.954$, again below the steady detonation shock pressure $P = 1$. The pressure and density change within the induction zone begins to decline as the chain-branching induction zone becomes longer, indicating that the strength of the expansion wave has declined. The reaction zone has now fallen significantly back from the shock as the maximum rate of radical production falls below that for location 5. The peak radical concentration has a value $y = 0.608$ at $x = -1.94$. The detonation structure now begins to resemble that associated with the steady structure for a lower T_{B} than for $T_{\mathrm{B}} = 0.82$. The pressure drop through the main reaction layer also declines but the density drop remains significant. As the weakening expansion wave further erodes the shock, the reaction zone further drops away from the shock as the length of the chain-branching induction zone increases, while the chain-termination region decreases. This continues until the pressure and density are almost constant in the induction zone and the detonation shock pressure attains a minimum once again, corresponding to the profiles observed at location 1 in the cycle. Thereafter, the cycle is repeated.

In summary, for a chain-branching cross-over temperature $T_{\mathrm{B}} = 0.82$, the detonation shock is observed to undergo a longitudinal pulsating instability with a constant amplitude and frequency. The mechanisms behind this so-called regular mode of instability have been revealed in figure 3. At a minimum point in the shock pressure cycle, the reaction zone lies further behind the shock than is found for the steady detonation profile for $T_{\mathrm{B}} = 0.82$, while the pressure drop through the reaction is small. The variations in pressure and density in the induction zone are almost uniform. A finite-amplitude compression wave with a wavelength commensurate with the length of the chain-branching induction zone then amplifies the shock, decaying as a maximum point in the pressure cycle is reached. The main reaction zone is drawn close to the detonation shock and the detonation adopts the structure of a steady detonation with a lower value of T_{B} than $T_{\mathrm{B}} = 0.82$. Since chemical reaction can no longer sustain further increases in the shock pressure, an expansion wave with a wavelength commensurate with the length of the chain-branching induction zone then causes a decay in the shock strength causing the reaction layer to drop away from the shock. The peak concentration of radical in the structure also decays until a minimum point in the cycle is again attained. The instability mechanism is thus dominated by finite-amplitude compression and expansion waves that appear between the detonation shock and reaction zone, while the maximum and minimum points in the profile correspond to almost uniform variations of pressure and density through the chain-branching induction zone.

(*b*) *Large-amplitude mode: chain-branching cross-over temperature* $T_{\mathrm{B}} = 0.86$

Figure 4 shows the shock pressure history for $T_{\mathrm{B}} = 0.86$. A linear stability analysis establishes the presence of three unstable modes with the most dangerous being a low-frequency mode with a growth rate $\mathrm{Re}(\alpha_1) = 0.0504$ and period $T = 59.61$. Figure 4 shows two types of pressure oscillations, one of large amplitude and short duration, the second of smaller amplitude but longer duration. A feature of pressure trace at $T_{\mathrm{B}} = 0.86$ are the long periods of nearly uniform pressure preceding the large-amplitude jumps. Precisely this mode of instability is observed experimentally, and

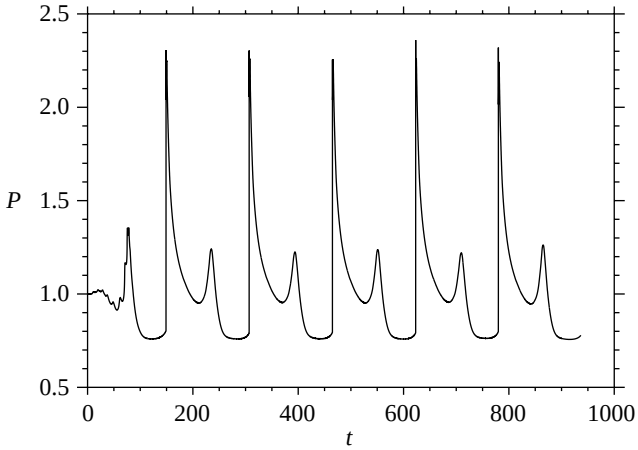

Figure 4. Shock pressure history for $T_{\mathrm{B}} = 0.86$.

is referred to as the large-amplitude mode by Alpert & Toong (1972). The steady wave structure is characterized by a longer temperature-sensitive chain-branching induction zone than that present for $T_{\mathrm{B}} = 0.82$.

Figure 5*b–e* reveals the mechanisms underlying the large-amplitude pressure pulse in figure 4. Location 1 in figure 5*a* indicates the point at which the location of the peak radical concentration lies furthest from the shock front (cf. location 1 in figure 3*a*). The detonation structure at this location consists of a long chain-branching induction period in which the pressure and density profiles are almost uniform. The reaction zone structure is characterized by a large variation in density, with the pressure varying only slightly. The radical peak concentration is given by $y = 0.371$ at $x = -13.65$, compared with a peak $y = 0.534$ at $x = -2.65$ for the steady detonation wave structure for $T_{\mathrm{B}} = 0.86$ (figure 1*a*). Thus the reaction zone lies over five times further from the shock than in the steady wave. The peak of radical production is given by $r_{\mathrm{I}} + r_{\mathrm{B}} - r_{\mathrm{C}} = 0.254$ at $x = -13.40$. The shock pressure is given by $P = 0.762$, having an instantaneous Mach number $D = 2.148$. Once again this structure has common links with the low-Mach-number fast-flame structures described by Clarke (1983) and Kassoy & Clarke (1985).

At location 2, a finite-amplitude wave of compression is observed to form ahead of the reaction zone as the reaction zone accelerates towards the shock. At this time, the peak radical concentration is $y = 0.567$ at $x = -10.85$. However, unlike the situation described for $T_{\mathrm{B}} = 0.82$, the compression wave does not extend the length of the chain-branching induction zone, but is localized in a region towards the reaction zone. The pressure and density profiles near the shock are still fairly uniform, and there is only an incremental rise in the shock pressure. The compression wave continues to steepen, and at location 3 a shock wave has developed. The compression wave drives the reaction zone with it, and at location 3 the initial birth of an internal detonation is observed. During this time, the lead detonation shock pressure remains almost fixed. The shock continues to grow in amplitude driven by the chemical reaction, and location 4 shows the internal shock and reaction zone complex prior to collision with the lead detonation shock. The internal shock amplitude is characterized by a pressure jump $P = 1.42$, stronger than the lead detonation shock. The sequence 1–4 is

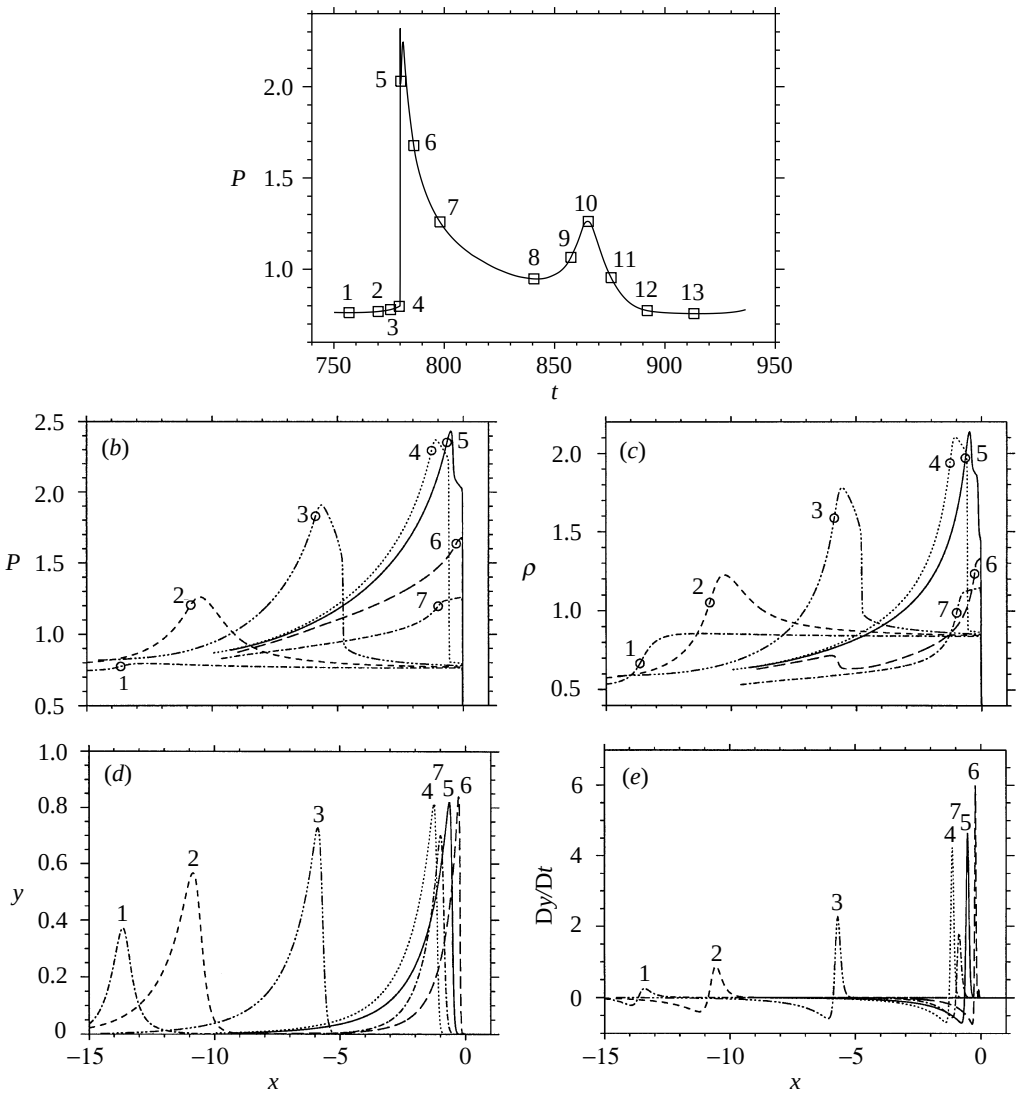

Figure 5. Snap-shot profiles of the mechanisms underlying the large pressure mode found in the detonation shock pressure trace for $T_{\mathrm{B}} = 0.86$ for (*b*) pressure, (*c*) density, (*d*) radical concentration and (*e*) radical production rate in a frame of reference attached to the detonation shock. Labels 1–7 in (*a*) show the points in the detonation shock pressure cycle at which the snapshots are taken. For clarity, corresponding curves are also shown in a different linetype. The circles in (*b*) and (*c*) correspond to points of peak radical concentration.

very reminiscent of the process of transition to detonation observed in the detonation initiation studies of Clarke *et al.* (1986, 1990), Sileem *et al.* (1991) and Dold *et al.* (1995). Here, though, the process can be thought of as a fast-flame-to-detonation transition and plays an integral part of the large-amplitude detonation instability mechanism.

Location 5 shows snapshot profiles after the shock collision and prior to a reignition event at the contact surface generated in the collision process. The collision leads to a

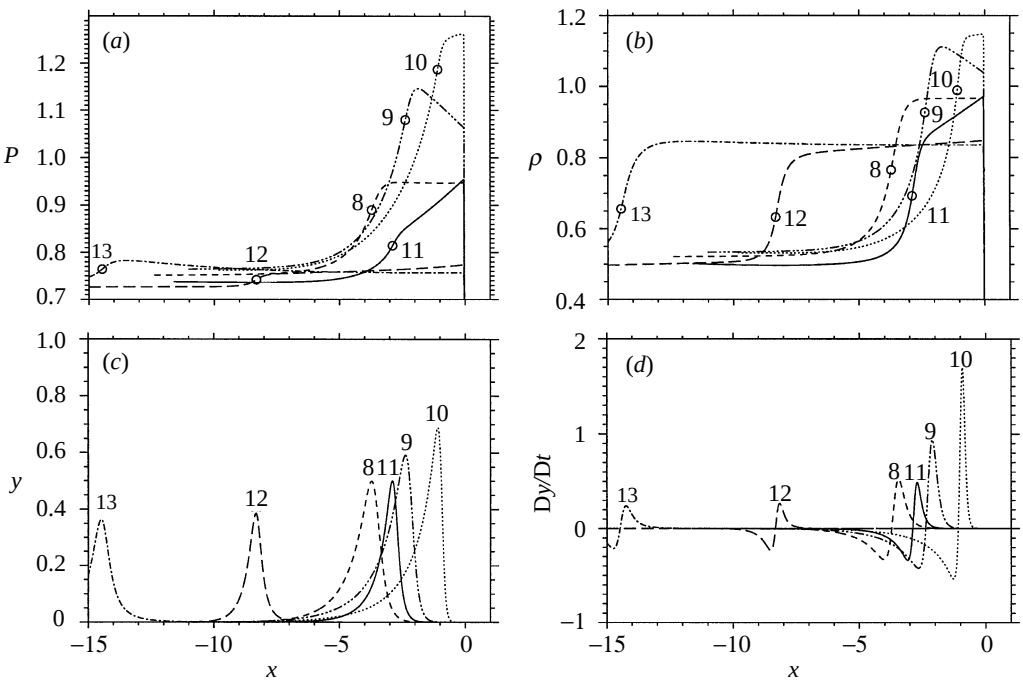

Figure 6. Snap-shot profiles of the mechanisms underlying the weak pressure mode found in the detonation shock pressure trace for $T_{\mathrm{B}} = 0.86$ for (*a*) pressure, (*b*) density, (*c*) radical concentration and (*d*) radical production rate in a frame of reference attached to the detonation shock. The labels 8–13 in figure 5*a* show the points in the detonation shock pressure cycle at which the snapshots are taken. For clarity, corresponding curves are also shown in a different linetype. The circles in (*a*) and (*b*) correspond to the points of maximum radical concentration.

single shock having $P = 2.02$ immediately after collision, and accounts for the large-amplitude mode observed in the experiments. The collision process and reignition event are studied in more detail by Dold *et al.* (1995). Following the interaction, a strong expansion wave begins to erode the lead shock, and its strength quickly diminishes. Locations 6 and 7 show snapshot profiles of the erosion process and the response of the reaction layer during the decay. At location 6 the shock has a peak $P = 1.67$, sufficiently strong that the chain-branching induction zone is very short and the reaction zone is located almost immediately behind the shock. The peak radical concentration is given by $y = 0.839$ at $x = -0.28$. The erosion of the shock continues at a slower rate, and as seen in the snapshot profiles corresponding to location 7, the chain-branching induction zone begins to lengthen, while the density and pressure begin to flatten in this zone.

The shock decay occurs until location 8 is reached in figure 5*a*. Snap-shot profiles corresponding to location 8 are shown in figure 6. At this location, the density and pressure profiles are again uniform in the chain-branching induction zone, while substantial drops in pressure and density occur through the reaction layer. The peak radical concentration is given by $y = 0.499$ at $x = -3.72$, compared with $y = 0.534$ at $x = -2.65$ in the steady wave for $T_{\mathrm{B}} = 0.86$ (figure 1). The profiles corresponding to locations 9–11 reveal the mechanisms behind the smaller-amplitude pressure pulse observed in figure 5*a*. The mechanisms are very similar to those observed for

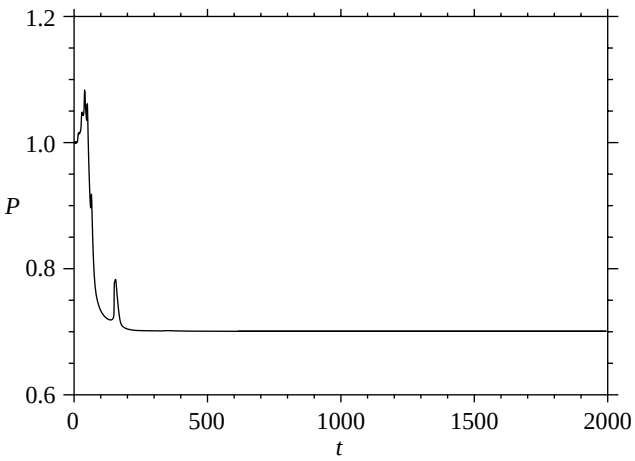

Figure 7. Shock pressure history for $T_{\mathrm{B}} = 0.89$.

the regular pulsations seen for $T_{\mathrm{B}} = 0.82$ (figure 3) and so no further descriptions are required, except to comment on one major difference between the two. During the decay stage of the cycle, the expansion wave continues to erode the shock pressure past that present at location 8 for the start of the smaller-amplitude pressure pulse. Even at location 11, where the shock pressure is close to that of location 8, substantial expansion processes are still present in the chain-branching induction zone. This feature is likely to be related to the region of pressure variation through the reaction zone at location 8. For the regular oscillatory cycle observed for $T_{\mathrm{B}} = 0.82$, the start of the cycle has only a small pressure variation through the reaction zone. In contrast the region of pressure drop for location 8 appears to allow the continued erosion of the shock past that present at location 8 during the decay cycle. The erosion of the shock continues, and uniform variations of the density and pressure once again begin to appear in the chain-branching induction zone, as can be observed at location 12. While a substantial density drop through the reaction layer is maintained as the reaction layer recedes from the shock, the pressure drop diminishes, and at the end of the cycle, location 13, the structure of a low-Mach-number fast flame is again recovered before the cycle repeats.

Figures 5 and 6 have revealed the mechanisms behind the mode of instability referred to by Alpert & Toong (1972) as the large-amplitude mode. In the experiments, the large-amplitude mode is often associated with irregular pulsations of the detonation front, precisely the scenario observed for $T_{\mathrm{B}} = 0.86$. The large-amplitude pressure pulse observed in figure 4 is associated with the formation of an internal detonation via an apparent fast-flame-to-detonation transition process. The internal detonation overtakes the original lead detonation shock, the interaction generating the very large pressure amplitude observed. The new detonation shock rapidly decays before a smaller pressure pulse occurs, whose mechanisms are similar to the regular oscillatory pressure pulse observed for $T_{\mathrm{B}} = 0.82$. The major difference is that during the decay stage of the smaller-amplitude pulse, the expansion continues to erode the shock until the fast-flame reaction zone structure is recovered and the cycle repeats.

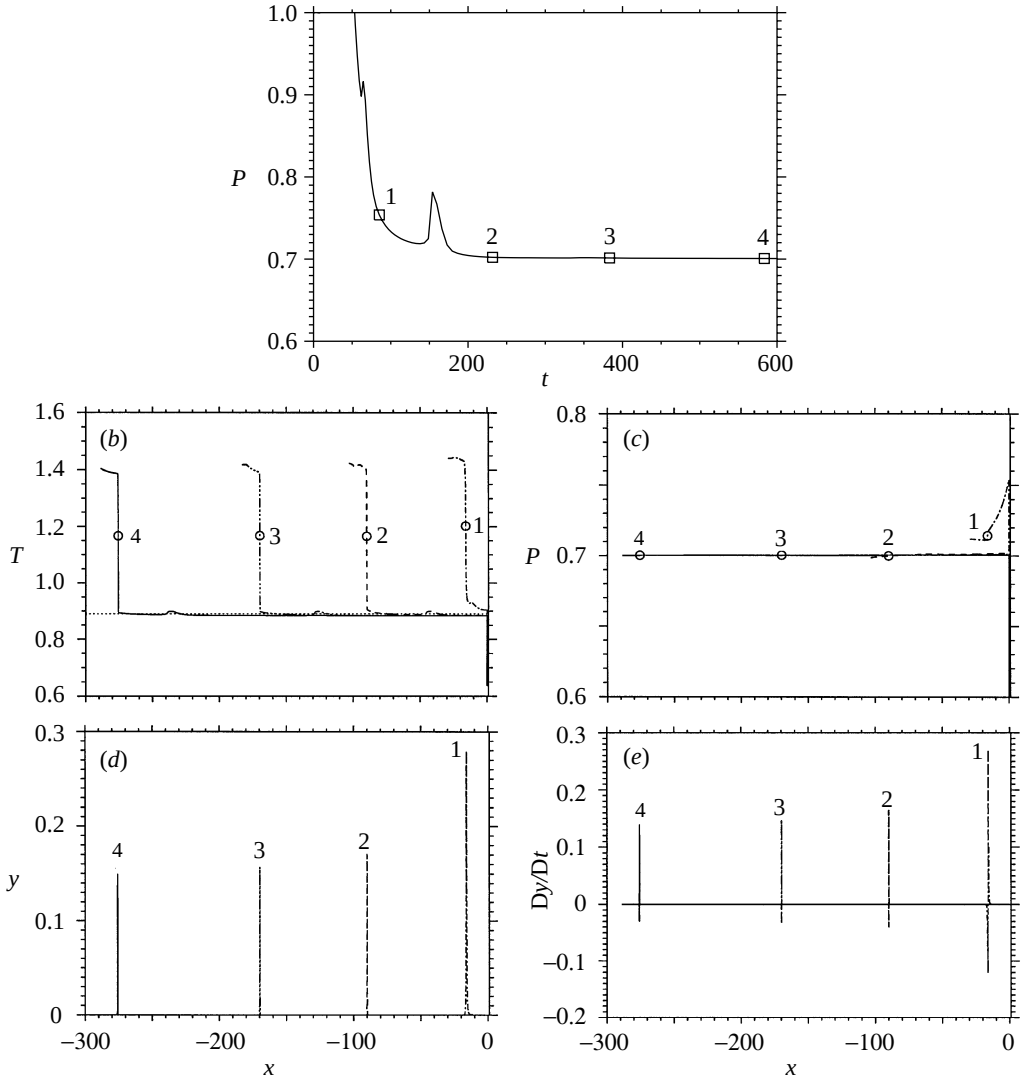

Figure 8. Snapshot profiles of the flame receding from the detonation front during detonation failure for $T_{\mathrm{B}} = 0.89$ for (b) temperature, (c) pressure, (d) radical concentration and (e) radical production rate in a frame of reference attached to the detonation shock. The labels in (a) show the points in the detonation shock pressure cycle at which the snapshots are taken. For clarity, corresponding curves are also shown in a different linetype. The circles in (b) and (c) correspond to the points of peak radical concentration. The dotted line in (b) indicates the value of the chain-branching cross-over temperature $T_{\mathrm{B}} = 0.89$.

(c) *Detonation failure: chain-branching cross-over temperature* $T_{\mathrm{B}} = 0.89$

Figure 7 shows the pressure trace associated with a chain-branching cross-over temperature $T_{\mathrm{B}} = 0.89$, illustrating a case of detonation quenching. Figure 8 reveals the mechanisms leading to the failure of the detonation. Location 1 corresponds to a point in the decay cycle of the detonation front, after the initial growth from

$t = 0$. Here the shock pressure is given by $P = 0.753$. As before, an expansion wave is observed in the chain-branching induction zone, indicating further decay of the shock front is taking place. The peak radical concentration is given by $y = 0.279$ at $x = -16.03$. For $T_{\mathrm{B}} = 0.82$ and $T_{\mathrm{B}} = 0.86$, this decay stage ultimately gives way to a growth stage and an oscillatory cycle is established. At location 2, however, the expansion wave has reduced the shock temperature $T = 0.884$ to marginally below that of the chain-branching cross-over temperature $T = 0.89$. The reaction zone, characterized by a peak radical concentration $y = 0.170$ at $x = -89.87$, has retreated markedly from the shock and the reaction zone and shock are effectively decoupled. The snapshots at locations 3 and 4 illustrate that this trend continues as time progresses. At location 3 the peak radical concentration is $y = 0.157$ at $x = -169.77$, while at location 4 it is $y = 0.149$ at $x = -275.65$. At $t = 2000$, the reaction zone is still retreating from the shock, and we conclude that the detonation has failed. The explanation for the failure is given in Short & Quirk (1997) as follows: when the shock temperature falls to the chain-branching cross-over temperature, the concentration of chain-radicals can then only accumulate at the exponentially small rate k_{I}. The rapid acceleration in concentration of chain-radicals brought about by the presence of the exponentially large rate constant k_{B} in the chain-branching reaction no longer occurs. Under these circumstances, the reaction zone drops to an exponentially large distance behind the shock. Since the energy of chemical reaction arising from within the reaction zone is required to drive the detonation, the detonation is effectively quenched. The retreat of the reaction zone from the shock, and the detonation failure, when the shock temperature drops below the chain-branching cross-over temperature is clearly demonstrated in figure 8. Although we associate this scenario with detonation failure, it should be noted that, in principle, a detonation could reappear after an exponentially long time at an exponentially large distance from the shock front that is not worth calculating, and external losses, such as heat or momentum losses, would be required to ensure a definite permanent form of failure.

4. Summary

The hydrodynamic mechanisms behind the regular and irregular modes of pulsating detonation-wave instability and behind the failure of a one-dimensional detonation wave observed in experiments have been revealed by direct numerical simulation. Regular oscillations are observed to be driven by low-frequency finite-amplitude compression and expansion waves travelling between the main reaction layer and the shock. Irregular oscillations involve a decoupling of the main reaction layer from the detonation front, an acceleration of the main reaction layer and a transition to detonation. The internal detonation wave overtakes the lead detonation shock, generating a new detonation with a large overpressure, which rapidly decays. A smaller-amplitude pressure oscillation occurs during the decay with a mechanism reminiscent of that observed for the previous regular oscillation, before the detonation and main reaction layer once again decouple and the instability cycle is repeated. For failure scenarios, the shock temperature is observed to drop to the cross-over temperature for the chain-branching reaction, causing the main reaction layer to decouple and retreat indefinitely from the detonation shock. The authors have also established that similar mechanisms for the regular and irregular modes of instability found for

the present three-step reaction model also apply to the pulsating detonation instabilities found for the standard one-step reaction model (Fickett & Wood 1964; Bourlioux *et al*. 1991; Quirk 1994). However, a major drawback of the one-step reaction model is its inability to define the notion of a detonability limit. The present study also highlights the need for more studies of fast flames to be made in order to understand completely the pulsating detonation instability.

M.S. was supported by the US Air Force Office of Scientific Research, Mathematics (F49620-96-1-0260). A.K.K. was supported by the Los Alamos National Laboratory and by the National Science Foundation.

References

Alpert, R. L. & Toong, T. Y. 1972 Periodicity in exothermic hypersonic flows about blunt projectiles. *Astronaut. Acta* **17**, 538–560.

Behrens, H., Struth, W. & Wecken, F. 1965 Studies of hypervelocity firings into mixtures of hydrogen with air or oxygen. In *10th Symp. (Int.) on Combustion*, pp. 245. Pittsburgh, PA: The Combustion Institute.

Bourlioux, A., Majda, A. J. & Roytburd, V. 1991 Theoretical and numerical structure for unstable one-dimensional detonations. *SIAM Jl Appl. Math.* **51**, 303–343.

Cheryni, G. G. 1968 Supersonic flow past bodies with formation of detonation and combustion fronts. *Astronaut. Acta* **13**, 467–475.

Clarke, J. F. 1983 On Changes in the structure of steady flames as their speed increases. *Combust. Flame* **50**, 125–138.

Clarke, J. F., Kassoy, D. R. & Riley, N. 1986 On the direct initiation of a plane detonation wave. *Proc. R. Soc. Lond.* A **408**, 129–148.

Clarke, J. F., Kassoy, D. R., Meharzi, N. E., Riley, N. & Vasantha, R. 1990 On the evolution of plane detonations. *Proc. R. Soc. Lond.* A **429**, 259–283.

Dold, J. W., Short, M., Clarke, J. F. & Nikiforakis, N. 1995 Accumulating sequence of ignitions from a propagating pulse. *Combust. Flame* **100**, 465–473.

Fickett, W. & Davis, W. C. 1979 *Detonation*. University of California Press.

Fickett, W. & Wood, W. W. 1964 Flow calculations for pulsating one-dimensional detonations. *Phys. Fluids* **9**, 903–916.

Glaister, P. 1988 An approximate linearized Riemann solver for the Euler equations for real gases. *J. Comp. Phys.* **74**, 382–408.

Kaneshige, M. J. & Shepherd, J. E. 1996 Oblique detonation stabilized on a hypervelocity projectile. In *26th Symp. (Int.) on Combustion*, pp. 3015. Pittsburgh, PA: The Combustion Institute.

Kassoy, D. R. & Clarke, J. F. 1985 The structure of a steady high-speed deflagration with a finite origin. *J. Fluid. Mech.* **150**, 253–280.

Lehr, H. F. 1972 Experiments on shock-induced combustion. *Astronaut. Acta* **17**, 589–597.

McVey, J. B. & Toong, T. Y. 1971 Mechanism of instabilities of exothermic hypersonic blunt-body flows. *Combust. Sci. Tech.* **3**, 63–76.

Quirk, J. J. 1994 Godunov-type schemes applied to detonation flows. In *Combustion in high-speed flows* (ed. J. Buckmaster, T. L. Jackson & A. Kumar), pp. 575–596. Kluwer.

Quirk, J. J. 1996 A parallel adaptive mesh refinement algorithm for computational shock hydrodynamics. *Appl. Numer. Math.* **20**, 427–453.

Reugg, F. W. & Dorsey, W. W. 1963 In *9th Symp. (Int.) on Combustion*, p. 476. Pittsburgh, PA: The Combustion Institute.

Saint-Cloud, J. P., Guerraud, Cl., Brochet, C. & Manson, N. 1972 Some properties of very unstable detonations in gaseous mixtures. *Astronaut. Acta* **17**, 487–498.

Short, M. & Dold, J. W. 1996 Unsteady gasdynamic evolution of an induction domain between a contact surface and a shock wave. I. Thermal runaway. *SIAM Jl Appl. Math.* **56**, 1295–1316.

Short, M. & Quirk, J. J. 1997 On the nonlinear stability and detonability limit of a detonation wave for a model 3-step chain-branching reaction. *J. Fluid. Mech.* **339**, 89–119.

Sileem, A. A., Kassoy, D. R. & Hayashi, A. K. 1991 Thermally initiated detonation through deflagration to detonation transition. *Proc. R. Soc. Lond.* A **435**, 459–482.